Effects of Non-Uniform Beam-Filling on Rainfall Retrieval for the TRMM Precipitation Radar

S. L. Durden, Z. S. Haddad, A. Kitiyakara, and F. K. Li

Jet Propulsion Laboratory
California Institute of Technology

To be submitted to: *J. Atmos. Oceanic Tech.*

Abstract

The Tropical Rainfall Measuring Mission (TRMM) will carry the first spaceborne radar for rainfall observation. Because the TRMM Precipitation Radar (PR) footprint size of 4.3 km is greater than the scale of some convective rainfall events, there is concern that non-uniform filling of the PR beam may bias the retrieved rain rate profile. We investigate this effect using data from the NASA/JPL Airborne Rain MApping Radar (ARMAR) acquired during TOGA COARE in early 1993. Our approach is to simulate TRMM PR observations using the ARMAR data and compared the retrieved rain rate from the simulated PR with the average rain rate obtained from the high resolution radar measurements. We find that the rainrate is overestimated somewhat near the top of the rainfall column and can be severely underestimated near the surface. It appears that NUBF effects can be reduced by using simple correction procedures.

1 Introduction

Spaceborne measurement of precipitation, especially over the tropical oceans, is important for understanding of atmospheric dynamics and climate. Passive microwave sensors have already been used for this application (Ferraro et al. 1996). Because the lower frequency microwave radiometers have footprints with diameters up to tens of km, rainfall parameters can vary within the footprint. Such non-uniform beam-filling (NUBF) can cause biases in the estimated rainfall parameters (Graves 1993, Ha and North 1995). The passive retrieval algorithm of Kummerow and Giglio (1994) includes a technique to correct for NUBF effects. Observation of precipitation in the tropics will be substantially enhanced by the launch of the Tropical Rainfall Measuring Mission (TRMM) in the late 1990's (Simpson et al. 1988). In addition to passive instruments, TRMM will carry the first spaceborne radar for rainfall observation. This instrument, the Precipitation Radar (PR), will be used to create rainfall profiles and monthly surface rainfall rate averages. The PR footprint at nadir is 4.3 km, and achievement of a smaller footprint would have required a higher frequency, a larger antenna, or a lower altitude. Each of these choices would have produced undesirable effects, including higher rainfall attenuation, increased mass and blockage of other instruments' field of view, and reduced mission lifetime. Future spaceborne rain radars will likely face similar constraints and can also be expected to have footprints with diameters of more than 1 km. While a footprint size of several kilometers is excellent compared to lower frequency microwave radiometers, it is still larger than the scale over which rainfall parameters can vary. Goldhirsh and Musiani (1986), for example, found that the median convective cell size for convective storms off the Virginia coast is 1.9 km. Consequently, it is possible that NUBF could cause biases in TRMM PR measurements, as well as future systems with several kilometer resolution.

Previous work on this problem includes the study of Nakamura (1991), who found biases for both simple rainfall models and real data derived from ground-based radar observations. He evaluated the retrieval bias for different resolutions and different retrieval algorithms. Amayenc et al. (1993) evaluated NUBF bias effects using simulated radar data, and Amayenc et al. (1996) evaluated NUBF bias using data from a nadir-looking aircraft radar for a rain storm off the U.S. Atlantic coast. Testud et al. (1996) used both simulation and ground-based radar data for a convective rainfall case to evaluate NUBF effects. They also noted biases in the retrieved rain rate. Kozu and Iguchi (1996) proposed an algorithm for correcting biases due to NUBF and evaluated the algorithm using ship-based radar data.

The purpose of this paper is to report investigations into the statistical nature of NUBF effects using a large data set acquired by the NASA/JPL Airborne Rain MApping Radar (ARMAR) during the Tropical Oceans Global Atmosphere Coupled Ocean Response Experiment (Lukas and Webster 1992). Data from ARMAR is ideal for such a study because it operates with the same frequency and downward-looking geometry as the TRMM PR but has substantially better spatial resolution (800 m at the surface). The ARMAR TOGA COARE dataset is ideal for TRMM PR studies because it consists of extensive measurements of ocean mesoscale convective systems, which are expected to be typical of the type of rainfall that TRMM will observe. The methodology for this study consists of simulating the TRMM PR using the ARMAR TOGA COARE data, retrieving rainfall rate from the simulated PR data, and comparing the result with rain rates retrieved from the higher horizontal resolution ARMAR data. This study differs from previous work in its use of data at the TRMM PR frequency and in the volume of data used, allowing NUBF bias

be used, and a technique for obtaining such a measurement is the Surface Reference Technique (SRT), first proposed by Meneghini et al. (1983). In the SRT a radar measurement of the ocean surface in a clear area is compared with the measurement in the raining area. The difference in the measurements is assumed to be due only to the rainfall attenuation and is taken to be the two-way PIA. The SRT-measured PIA is then used as a constraint; the attenuation correction at the surface is made to equal that measured by the SRT. The SRT forms the basis of the TRMM PR algorithm (denoted 2A25); however, the TRMM algorithm also includes techniques for NUBF correction (described in part in Kozu and Iguchi 1996) and for handling light rain, where the relative error in the SRT-measured PIA can be large (Iguchi and Meneghini 1994). Marzoug and Amayenc (1994) have also considered algorithms similar to the the Hitschfeld-Bordan algorithm in combination with the SRT-measured PIA.

While details of the aforementioned algorithms vary, they are similar in principle. First,.the SRT is used to estimate the PIA and develop corrections to the initial algorithm assumptions about the $k-R$ or $Z-R$ relations. Next, the retrieval process begins either at the top of the rain and works downward or at the surface and works upward. The measurement at each range bin is corrected for attenuation using the results from the previous range bins. All the algorithms were derived assuming that the rain within the resolution cell is uniform. When rainfall is not uniformly distributed, one would like to retrieve the rain rate averaged over the resolution cell. Obviously, this could be done using algorithms derived for the uniform case if the measured PIA and reflectivity profile were those corresponding to the profile of average rain rate within the beam. Unfortunately, because of the nonlinearity in the relations between reflectivity, attenuation, and rain rate, the measured reflectivity profile and PIA may deviate from those corresponding to the average rain rate. The method of Kozu and Iguchi (1996) uses the observed PIA and its variability to estimate the PIA that corresponds to the average rain rate.

To understand the effects of NUBF, we can thus compare not only the rain rate retrieved from a spaceborne system with the average rain rate but also the observed PIA and reflectivity profile with those corresponding to the average rain rate profile. To see how NUBF can effect the PIA and reflectivity profile observations, consider a two-dimensional slice of the atmosphere that has the width of a radar beam and the height L of a typical storm (Figure 1). Assume that this region can be segmented into a uniform grid of boxes whose dimensions are small enough that the rain rate can be considered uniform within each box. As noted previously, when the rain rate is not distributed uniformly throughout the radar resolution volume, the quantity to be retrieved is the horizontally averaged rain rate, i.e., $\frac{1}{M}\sum_{j=1}^{M} R_{i,j}$. where $R_{i,j}$ is the rain rate within the $(i,j)^{th}$ box of the $M \times N$ grid $1 \leq j \leq M$, $1 \leq i \leq N$. The two-way PIA corresponding to the horizontally averaged rain rate is

$$A_t = 10^{-0.2\frac{L}{N}\sum_{i=1}^{N}\alpha\left(\frac{1}{M}\sum_{j=1}^{M}R_{i,j}\right)^{\beta}} \tag{4}$$

where the subscript t denotes "true". However, if one divided the echo power received from the surface within this region by the power received from the surface under clear air (as done in the SRT), the apparent attenuation A_a that one would obtain (assuming a rectangular antenna gain pattern) should be equal to

$$A_a = \frac{1}{M}\sum_{j=1}^{M}\left(10^{-0.2\frac{L}{N}\sum_{i=1}^{N}\alpha R_{i,j}^{\beta}}\right) \tag{5}$$

where the subscript a denotes "apparent". Because of the non-linear dependence of attenuation on R, A_t and A_a are generally not equal. In a simple example in which the beam is half-filled with rain and half clear, Nakamura (1991) noted that the maximum observed PIA is 3 dB. However, the "true" PIA, which corresponds to the average rain rate, can be much larger. Thus, the PIA and the path-averaged rain rate (PARR) can be severely underestimated.

Next, we consider the effect of non-uniformity on the reflectivity. Near the top of the rain column, attenuation can be neglected, and the apparent reflectivity, as measured by the spaceborne radar, would be

$$Z_a = \frac{1}{M}\sum_{j=1}^{M} aR_{i,j}^{b} \tag{6}$$

statistics to be derived. We begin by presenting a brief discussion of the ARMAR TOGA COARE data set. This is followed by a review of rain retrieval theory and a theoretical discussion of the NUBF problem. The simulation technique and errors due to NUBF are then presented.

2 TOGA COARE Data Characteristics

TOGA COARE was an international field experiment carried out in the Western Pacific Ocean in 1992-93. The NASA DC-8 aircraft flew a total of 13 TOGA COARE missions in January and February 1993. It was equipped with the ARMAR radar system, as well as various microwave radiometers, and infrared and optical instruments. ARMAR was designed to support the TRMM PR instrument development and algorithm development. It operates at the PR frequency of 13.8 GHz (Ku-band) and uses a scanning geometry similar to the PR, scanning its antenna across-track $\pm 20^o$. Unlike the PR, it has Doppler and multi-polarization capabilities. It also functions simultaneously as a radiometer, acquiring the 13.8 GHz brightness temperature. Calibration of the reflectivity was accomplished using a calibration loop, which couples a portion of the transmitted power to the receiver (Durden et al. 1994). Calibration was verified by examining the measured ocean backscatter cross section σ^o at 10° incidence under clear conditions. ARMAR characteristics are shown in Table 1, along with the corresponding characteristics of the PR. Additional details on ARMAR hardware and data processing can be found in Durden et al. (1994).

During TOGA COARE, most of the precipitation observed by ARMAR was associated with mesoscale convective systems (MCSs). As discussed by Houze (1981) precipitation can be classed as either stratiform or convective. Convective rainfall is produced in regions of intense updrafts and downdrafts. It is characterized by high rain rates and large horizontal variability. Stratiform rain, on the other hand, is associated with areas of weak vertical motion and is produced as ice particles sink and melt. Stratiform rain is usually much lighter, much more spatially uniform, and more spatially extensive than convective rain. In radar imagery it can typically be recognized by the presence of a region of high reflectivity, called the bright band, located just below the 0° C isotherm. For stratiform rain the correlation length in the horizontal direction is typically many kilometers, as observed in the ARMAR data. In intense convective events, by contrast, the rainfall rate is highly variable and the correlation length can be less than the 4.3 km size of the TRMM PR footprint. Thus, it is primarily convective rain in which effects of NUBF are expected to cause problems.

3 Theory of NUBF Effects

To appreciate the possible problems caused by NUBF, it is necessary to review the pertinent aspects of radar rain fall measurement. At lower frequencies (e.g., 3 GHz) attenuation due to rainfall is generally small and the rainfall rate has typically been retrieved from radar observations using $Z - R$ relations, which relate the radar reflectivity factor Z to the rainfall rate R by a power law $Z = aR^b$. However, at the higher frequencies typically used for airborne and spaceborne radars, attenuation is larger and cannot be neglected. In this case the measured reflectivity Z_m is related to the reflectivity Z by

$$Z_m(r) = Z(r)10^{-0.2\int_0^r k(s)ds} \tag{1}$$

where r is range and k is the specific attenuation. Recovery of both the Z and k profiles given only Z_m is underdetermined. However, by assuming a $k - R$ relation of the form $k = \alpha R^\beta$, as well as a $Z - R$ relation, 1 can be solved analytically for $R(r)$ given $Z_m(r)$ (Hitschfeld and Bordan 1954). In this study we use the $Z - R$ and $k - R$ relations from Nakamura et al. (1990)

$$k = 0.032R^{1.124} \tag{2}$$

$$Z = 372.4R^{1.54} \tag{3}$$

As discussed by Hitschfeld and Bordan (1954) and Meneghini (1978) the solution of the radar equation 1 can be unstable unless an auxiliary measurement of rain rate or attenuation is used. For a downward-looking airborne or spaceborne radar an independent measurement of the path integrated attenuation (PIA) can

rate to also be slightly overestimated. Figure 2 (a) shows the PIA error versus rain rate; it can be seen that the PIA is always underestimated and that the error can become very large at high rain rates. The PARR derived from the PIA would also be underestimated. The error in the near-surface reflectivity, using equations 15 and 16, can be either positive or negative, as shown in Figure 2 (b). In evaluating 16, it was assumed that the means of R and R_p are equal. When the error in Figure 2 (b) is negative (underestimation), the surface rain rate will be underestimated, since it is derived from correcting the near-surface reflectivity by the apparent PIA, which is also underestimated. When the reflectivity is overestimated, the rain rate may be either underestimated or overestimated, depending on which error dominates (overestimation of reflectivity or underestimation of PIA). It can be seen in Figure 2 (b) the underestimation of reflectivity at high rain rates is more severe in the case where the near-surface and path-averaged rain rates are independent, given by 16.

4 Data Analysis Technique

To quantify the effects of NUBF on real radar data we need both spaceborne radar data and corresponding high resolution data for comparison. Currently, such data are not directly available, so we take the approach of simulating the spaceborne data using aircraft radar data, as was done by Amayenc et al. (1996). We simulate TRMM PR observations over these data in two steps. First, the ARMAR data is resampled to a uniform Cartesian grid; this is necessary because of aircraft motion, which cases the raw data to have non-uniform sampling. The resampling is performed by dividing the atmosphere in 60 m thick horizontal slices. The locations of the closest ARMAR measurements, along with the corresponding reflectivity are found for each slice. Thus, for each slice we have a set of reflectivity measurements specified by their reflectivity and location on the slice. We then construct a Delaunay triangulation and use linear interpolation to create a set of uniformly sampled reflectivities over each slice. The combination of all the horizontal slices gives a reflectivity volume with 60 m vertical spacing and 200 m horizontal spacing. The second step of the simulation involves convolving a multi-dimensional Gaussian function with the resampled data. The Gaussian is chosen so that it approximates both the range resolution (due to matched filtering in the receiver) and the two-way antenna pattern. One version of the simulation software uses a three-dimensional (3-D) Gaussian to simulate the TRMM PR resolution volume in the range direction and both the alon-track and cross-track dimensions. The other version uses a two-dimensional (2-D) Gaussian to simulate the PR range and along-track resolution. The overall simulation approach taken here is similar to the 2-D approach described in Amayenc et al. (1996), and the 3-D approach described in Testud et al. (1996).

In performing the convolution, there are several details to be considered. As discussed in Testud et al. (1996), a general simulation method must compute the attenuation to each range bin in the simulated spaceborne radar data. However, in our case ARMAR and the TRMM PR have the same geometry and frequency. Hence, the attenuation experienced by a simulated PR bin is essentially the same as the attenuation already experienced by the ARMAR measurement. Consequently, we do not need to explicitly include attenuation in the simulation procedure. The convolution is thus implemented directly on ARMAR reflectivity to produce the PR reflectivity. The TRMM reflectivity $Z_p r$ is given by

$$Z_{pr} = \frac{\int Z(r)W(r)\delta(r)dr}{\int W(r)\delta(r)dr} \tag{17}$$

where Z is the ARMAR reflectivity, $W(r)$ is the gaussian resolution function, r is the 2-D or 3-D spatial location, and the integrals are computed over the 2-D or 3-D space corresponding to the PR resolution volume. The function δ is an indicator function which takes on the value zero when ARMAR data is missing or invalid and unity when the ARMAR data is valid. This is useful in both the 2-D and 3-D codes when there are along-track gaps in the data due, for example, to a change in the radar mode. The indicator function is also needed in the 3-D code since ARMAR acquired data only over a relatively narrow $\pm 20^o$ range of scan angles. At the surface the ARMAR swath is more than twice the size of the PR footprint. However, at higher altitudes, the simulated PR footprint in the 3-D software may partially lie in areas with no ARMAR measurements.

When using a 3-D gaussian, it must be remembered that the ARMAR data used for a single TRMM PR footprint was acquired over approximately a 10° variation in the ARMAR antenna scan direction. For

However, the "true" reflectivity factor, corresponding to the horizontally averaged rain rate, is

$$Z_t = a\left(\frac{1}{M}\sum_{j=1}^{M} R_{i,j}\right)^b \tag{7}$$

These two quantities are, in general, equal only when there is not variation in R horizontally or when b is unity. Again using the simple example of a beam that is half-filled with rain and half clear, Nakamura (1991) found that the nonlinearity of the $Z - R$ relation causes the rain to be overestimated. Equivalently, Z_a is larger than Z_t.

For rain near the surface, attenuation cannot be neglected. In this case, the apparent reflectivity factor Z_a at range bin i is given by

$$Z_a = \frac{1}{M}\sum_{j=1}^{M} aR_{i,j}^b 10^{-0.2\frac{L}{N}\sum_{k=1}^{i}\alpha R_{k,j}^\beta} \tag{8}$$

while the modeled reflectivity factor using the horizontally-averaged rain rate is given by

$$Z_t = a\left(\frac{1}{M}\sum_{j=1}^{M} R_{i,j}\right)^b 10^{-0.2\frac{L}{N}\sum_{k=1}^{i}\alpha\left(\frac{1}{M}\sum_{j=1}^{M} R_{k,j}\right)^\beta} \tag{9}$$

As was the case for the PIA and unattenuated reflectivity, horizontal variability of R within the range bin can cause the apparent and true attenuated reflectivities, as defined by 8 and 9, to differ.

To perform a more quantitative analysis using the above equations, it is useful to view the rain rates in the ith range bin as being samples of a single random variable. In this case the averages over the locations within a single horizontal layer can be replaced by the statistical expectation E. The equations for the PIAs can then be written as

$$A_a = \mathcal{E}\left\{10^{-0.2L\alpha R_p^\beta}\right\} \tag{10}$$

$$A_t = 10^{-0.2L\alpha\mathcal{E}\{R_p\}^\beta} \tag{11}$$

where we use R_p to represent the path-averaged rain rate, or PARR. Near the top of the rain column, the reflectivities are

$$Z_a = a\mathcal{E}\{R^b\} \tag{12}$$

$$Z_t = a\mathcal{E}\{R\}^b \tag{13}$$

Near the surface the true reflectivity is

$$Z_t = a\mathcal{E}\{R\}^b 10^{-0.2L\alpha\mathcal{E}\{R_p\}^\beta} \tag{14}$$

The apparent reflectivity depends on the correlation between the surface rain rate and the PARR. For the case where they are perfectly correlated (i.e., R and R_p are equal)

$$Z_a = a\mathcal{E}\{R^b 10^{-0.2L\alpha R^\beta}\} \tag{15}$$

At the other extreme, if the surface rain rate and PARR are independent, the correct form for the apparent reflectivity is:

$$Z_a = a\mathcal{E}\{R^b\}\mathcal{E}10^{-0.2L\alpha R_p^\beta}\} \tag{16}$$

The rain rate over large areas has been found previously to satisfy the lognormal distribution (Lopez 1977, Kedem et al. 1990). The PIA, as measured by applying the SRT to ARMAR data, has also been found to satisfy the lognormal distribution (Tani and Amayenc 1995). Kozu and Iguchi (1996) assumed the lognormal distribution in developing their correction technique, althogh they found deviations from lognormal when considering the distribution of rainfall within a radar footprint. For this analysis we assume a lognormal PDF and compute the errors in the radar observables due to NUBF as a function of rain rate when the rain rate standard deviation is equal to one-half the rain rate mean. At the top of the rain column, where attenuation is negligible, the reflectivity is overestimated by 0.4 dB, independent of rain rate. This would cause the rain

rate is 21 mm/h. Figure 4 (b) shows the error (apparent minus true) in the PIA, near surface reflectivity, and 4 km reflectivity. The largest error is in the PIA, which is underestimated by nearly 4 dB in the convective cell. This is the primary source of error in the surface rain rate estimate. The reflectivity near the surface is slightly overestimated (0.4 dB), while the 4 km altitude reflectivity is overestimated by 1.7 dB.

Although studies of individual cases are useful, we choose, rather, to focus on statistics of NUBF biases over TOGA COARE, shown in Figure 5 and summarized in Table 2. Figure 5 (a) shows histograms of the errors in the radar observables, while Figure 5 (b) shows histograms of the rain rate errors. The number of occurences for each bin is plotted on a base-10 logarithm scale, since there a large number of small errors and only a small number of large errors. The total number of simulated PR footprints was 1779. The PIA error is (A_{ap}/A_t), while the PARR error is the apparent rain rate minus the true rain rate. The apparent quantities are always smaller than the true; i.e., a spaceborne radar would always underestimate PIA and PARR. The maximum error is 12 dB for the PIA and 21 mm/h for the PARR. If we compute the average rain rate over all 1779 footprints, we find that the apparent average is underestimated by 4.6%. The reflectivity and rain rate at 4 km altitude are always slightly overestimated. The maximum overestimations are 5.5 dB and 2.3 mm/h. In most cases, the overestimation is small; the average is overestimated by only 3.2%. The near-surface reflectivity errors are both negative and positive, extending from -12.2 dB to +10.4 dB; the mean is zero. The near-surface rain rate errors are more negative than positive and there are a few cases with errors as large as -79 mm/h. The maximum positive error is much smaller at approximately 18 mm/h. The average rain rate at the surface, computed over all 1779 footprints, is underestimated by 11%.

The histograms in Figure 5 show a large variability in the measurement errors. Presumably this is related to the variability of rainfall within the spaceborne radar's footprint. Figure 6 shows scatter plots of the measurement errors versus the standard deviation of the high resolution measurements within the footprint. In Figure 6 (a) the error in PIA is correlated with the standard deviation of the PIA with the PR footprint. Largest errors occur when the PIA variability is large. There is, however, significant scatter with large standard deviations sometimes producing fairly small errors, indicating that the error depends on other factors besides the standard deviation. One such factor is the mean PIA; in cases with large error, the mean PIA is also typically large. In Figure 6 (b) the error in the 4 km altitude reflectivity is correlated with the standard deviation of the high resolution 4 km altitude reflectivity. The near-surface reflectivity error (not shown) was found to be poorly correlated with both the PIA and near-surface reflectivity standard deviations.

6 Discussion

The observations presented in the previous section showed that the PIA and PARR are always underestimated, while the reflectivity and rain rate at 4 km altitude are always overestimated. This was also found in the model calculations presented in Section 3. The model calculations showed that for 50% variability in rainrate, the PIA could be underestimated by 7 dB at 50 mm/h and 25 dB at 100 mm/h. The largest observed PIA error is 12 dB, which is within the range predicted by the model for heavy rain. In contrast, the observed maximum error in rain-top reflectivity was 5.5 dB, as compared with the model calculation of 0.4 dB for a rain rate standard deviation of 50%. One reason that the predicted and observed errors differ more for rain-top reflectivity than PIA is that the PIA error is related to the variability of the PARR, while the reflectivity error is related to the variability of the rain-top rain rate. The variability of rain rate within individual layers can be greater than that for the PARR, as can be seen by considering rain with N layers, all with mean rain rate μ and standard deviation σ. If the layers are perfectly correlated, we can consider the rain to be acting as one layer with mean μ and standard deviation σ. On the other hand, if all layers are independent, the PARR still has mean equal to μ but standard deviation $\sigma/\sqrt{N}$. Thus, if the rain is behaving as several independent layers, for example, due to vertical shear of the horizontal wind, the standard deviation of the PARR would be lower than for that of the rain rate in the individual layers. Considering the data in Figure 6, the maximum relative standard deviation in PIA is about 125%. In contrast, the largest reflectivity standard deviation is about 400%.

Table 2 and Figure 5 (e) showed that the near-surface reflectivity can be under- or overestimated, with both types of error occurring frequently in the data. This is in agreement qualitatively with the model

backscatter from rain, this is probably not critical. However, for the ocean surface backscatter, the change over 10° can be an order of magnitude. Thus, the ocean backscatter must be first corrected to the PR incidence angle before the convolution. This is done by using the observations of ocean backscatter presented in Schroeder et al. (1985). This correction is not needed in the 2-D software. In both codes it is necessary to properly simulate speckle and thermal noise. ARMAR typically acquires $\geq$ 100 independent samples, several hundred in some modes. The PR, however, acquires 64 independent samples. This makes the PR fading noise greater than for ARMAR. In the simulation, additional fading noise is added. The PR thermal noise is also larger than for ARMAR, and appropriate thermal noise is also added.

Figure 3 shows an example of along-track reflectivity profile acquired by ARMAR and by the simulated TRMM PR, using the 2-D version of the simulation. To test the simulation procedure, we performed comparisons between the simulated data and ARMAR data for stratiform rain cases. We found that the reflectivities were very close ($\approx$ 1 dB). In completely uniform rain, they should be identical. We also used the ARMAR rather than PR parameters in the simulation and compared the results with the original ARMAR data. In all cases the two were very close.

For studying NUBF effects, we used only the 2-D version of the simulation to avoid assumptions about the ocean backscatter behavior. Furthermore, we limited the study to nadir and we did not add fading or thermal noise to the simulated PR data. The differences between the PR data and the high-resolution data are then due only to NUBF. The effect of NUBF is studied by comparing quantities derived from the simulated PR data with the same quantities derived from the average of the high resolution rain rate. So that the quantities can be directly compared, the averaging of the high resolution rain is performed over precisely the same antenna pattern as the reflectivity data, as was done by Amayenc et al. (1996). Vertical averaging of the ARMAR data to the PR range resolution is performed prior to rain retrieval so that the errors found in this study are due solely to horizontal variability of the rain. To test the procedure, comparisons were done for cases with highly uniform rain rates. In these cases the quantities being compared were essentially identical, providing confidence in the simulation and comparison procedure.

The quantities chosen for comparison are the true and apparent PIA, reflectivity just above the surface (500 m altitude), rain rate just above the surface (500 m altitude), reflectivity near the rain column top (4 km altitude), and rain rate near the rain column top (4 km altitude). The apparent PIA is derived by simply comparing the apparent surface reflectivity with the clear air value. The true PIA is derived by first computing the PIA for each high-resolution footprint, using the SRT. This is converted to the high-resolution PARR using the $k-R$ relation and then averaged over the PR footprint and converted back to the true PIA. The near-surface apparent reflectivity is that produced by the PR simulation. The near-surface apparent rain rate is found by correcting the apparent reflectivity by the apparent PIA and applying the $Z-R$ relation. The true reflectivity near the surface is the reflectivity corresponding to the average rain rate at the surface and attenuated by the attenuation corresponding to the path averaged rain rate. The reflectivities and rain rates near the rain column top are computed in the same manner as those near the surface, except that attenuation is neglected.

It should be pointed out that the rain retrieval algorithm used here is the simplest possible using the SRT-measured PIA. In our calculations the near-surface reflectivity is corrected by the measured PIA, as done in both kZS algorithm (Marzoug and Amayenc 1994) and the α-adjustment method used in the TRMM 2a25 algorithm (Iguchi and Meneghini 1994). However, we do not adjust the $k-R$ or $Z-R$ relations using the measured PIA. The relations used in all calculations are those given by 2 and 3, making our approach essentially that of the kZS algorithm. Our goal in making this choice was to test those features common to all SRT-based algorithms and to allow physical interpretation of the results.

5 Observations of NUBF Effects

We begin by considering the NUBF effects for the case displayed in Figure 3. This case consists of a rather strong convective cell at left, with lighter convective rain to the right. Figure 4 (a) compares the true and apparent surface rain rates. The apparent near-surface rain rate is similar to the true rain rate, except in the intense convective cell, where it is significantly smaller. There, the true is 36 mm/h, while the apparent rain

those corresponding to the horizontally averaged rain rate. We found that relative to the desired values, the PIA is always underestimated, the rain-top reflectivity is always overestimated, and the near-surface reflectivity is underestimated roughly as often as it is overestimated. The largest errors in magnitude occur for the near-surface rain rate; over TOGA COARE the average is underestimated by 11%. We found that the largest contributor to the rain rate error near the surface is the PIA error. A simple correction scheme for the PIA was found to reduce the bias.

Acknowledgment

The research described here was performed by the Jet Propulsion Laboratory, California Institute of Technology, under contract with the National Aeronautics and Space Administration. Support from the NASA TRMM Science program is gratefully acknowledged.

computations at the end of Section 3, where it was found that the reflectivity could be over- or underestimated. It was noted there that the rain rate error would depend on both the reflectivity error and the PIA error. Assuming that the PIA underestimation error is greater in magnitude than reflectivity overestimation, the rain rate would be underestimated. Underestimation of the near-surface rain rate, is, in fact, normally observed, although overestimation occurred in some cases. Our observations, therefore, indicate that the underestimation of the PIA is the primary source of bias in the near-surface rain rate. Also, it should be noted that an error in the PIA can cause a much larger error in the near-surface rain rate than the PARR. This is because the $k-R$ relation relates k in dB to R in mm/h. Hence, when the apparent PIA is 10 dB and the true is 20 dB, the PARR would be underestimated by around 50%. On the other hand, suppose that the near-surface Z is attenuated but otherwise correct. If we use the true PIA to compensate for attenuation, the result is a compensated Z that is 10 dB larger than when the apparent is used. The $Z-R$ relation is for Z in mm/h, not dBZ; hence, the resulting rain estimate can be more than an order of magnitude larger than for the case when the apprent PIA is used. This may explain the findings in Table 2, showing a maximum error of 20 mm/h in the PARR and a maximum of 79 mm/h for the near-surface rain rate. It is also likely the cause for the 11% underestimation in the average near-surface rain rate versus 5% underestimation of the average PARR, over TOGA COARE.

The seriousness of the errors shown in Figure 5 and Table 2 depends on the application. The really large errors are infrequent and do not greatly affect the estimates of average rain rate over the entire data set. The worst error was underestimation of the near-surface rainfall over TOGA COARE by 11%. Although small, such biases are undesirable; furthermore, if the application is a case study of a single mesoscale system, the bias can be quite large. Therefore, it is desirable to correct for NUBF effects so that the rain rate estimates are not biased. In general, a correction procedure has only the low-resolution data available and so must use these data to correct the spaceborne radar measurables, namely, the reflectivity profile and PIA.

Errors in the reflectivity near the top of the rain column are always positive but are fairly small. Errors in reflectivity near the surface are larger in magnitude but have mean of zero. Based on the radar equation 1, the behavior of the reflectivity error at arbitrary altitudes should be somewhere between these two extremes.

As discussed above, the most serious errors seem to be caused by the error in the PIA; correction of this error should be the first priority. A correction procedure for the PIA has been discussed in Kozu and Iguchi (1996), and as noted before such a procedure is planned for use in the TRMM PR retrieval algorithm. In Kozu and Iguchi (1996) the low-resolution PIA standard deviation is used to estimate the standard deviation of the rain rate within the radar footprint. The within-footprint standard deviation is then used to correct the path attenuation estimate. Figure 6 showed that the PIA is, indeed, related to the high-resolution PIA standard deviation. Although there is considerable scatter, the true PIA can be approximated by can be approximated by the quadratic

$$A_t = A_a + 0.1 - 0.43\sigma + 0.42\sigma^2 \tag{18}$$

Application of this equation to estimate the average rain rate over TOGA COARE reduced the bias in PARR from -5% to -0.3% and the bias in near-surface rain rate from -11% to +2%. This confirms that the PIA error is the dominant source of bias. Figure 7 shows the high-resolution PIA standard deviation versus the low-resolution standard deviation. The latter was estimated from only three samples since we have only along-track data; use of more than three samples covers a region more than 14 km long. This was thought to be too large for deriving the properties of rain within a single footprint. In Kozu and Ighuchi (1996) nine samples (three along-track and three cross-track) are used, providing a better estimate. In spite of the limitations, Figure 7 indicates that the low-resolution and high-resolution standard deviations are correlated, albeit weakly.

7 Conclusions

We have presented the results of a study of errors due to non-uniform beam-filling using a large data set of airborne radar data, collected awith the TRMM PR frequency and scanning geometry during TOGA COARE. We examined the errors in rain rate estimation and found similar results to previous studies: underestimation of the path-averaged rain rate (always) and near-surface rain rates (typically) and overestimation of the rain-rop rain rate (always). We also noted that the desired PIA and reflectivity profile are

Simpson, J., R. F. Adler, and G. R. North, 1988: A proposed tropical rainfall measuring mission (TRMM) satellite. *Bull. Am. Meteorol. Soc.*, 69, 278-295.

Tani, T., P. Amayenc, and M. Ali-Mehenni, 1995: Radar return from the ocean surface and path-integrated attenuation at 13.8 GHz as derived from ARMAR data in TOGA-COARE. *Proc. 27th Conf. on Radar Meteorlogy*, Vail, CO, Amer. Meteor. Soc.

Testud, J., P. Amayenc, X. K. Dou, and T. F. Tani, 1996: Tests of rain profiling algorithms for a spaceborne radar using raincell models and real data precipitation fields. *J. Atmos. Oceanic Technol.*, 13, 426-253.

Webster, P. J., and R. Lukas, 1992: TOGA COARE - The coupled ocean atmosphere response experiment, *Bull. Am. Met. Soc.*, 73, 1377-1416.

References

Amayenc, P., M. Marzoug, and J. Testud, 1993: Analysis of cross-beam resolution effects in rainfall rate profile retrieval from a spaceborne radar. *IEEE Trans. Geosci. Remote Sensing*, 31, 417-425.

Amayenc, P., J. P. Diguet, M. Marzoug, and T. Tani, 1996: A class of single-frequency algorithms for rain-rate profiling from a spaceborne radar. 2. Tests from airborne radar measurements. *J. Atmos. Oceanic Technol.*, 13, 142-164.

Durden, S. L., E. Im, F. K. Li, W. Ricketts, A. Tanner, and W. Wilson, 1994: ARMAR: An airborne rain mapping radar. *J. Atmos. Oceanic Technol.*, 11, 727-737.

Ferraro, R. R., F. Z. Weng, N. C. Grody, and A. Basist, 1996: An 8-year (1987-1994) time-series of rainfall, clouds, water-vapor, snow cover, and sea-ice derived from SSM/I measurements. *Bull. Amer. Meteor. Soc.*, 77, 891-905.

Goldhirsh, J., and B. Musiani, 1986: Rain cell size statistics derived from radar observations at Wallops Island, Virginia. *IEEE Trans. Geosci. Remote Sensing*, 24, 947-954.

Graves, C. E., 1993: A model for the beam-filling effect associated with the microwave retrieval of rain, *J. Atmos. Oceanic Technol.*, 10, 5-14.

Ha, E., and G. R. North, 1995: Model studies of the beam-filling error for rain-rate retrieval with microwave radiometers. *J. Atmos. Oceanic Technol.*, 12, 268-281.

Hitschfeld, W., and J. Bordan, 1954: Errors inherent in the radar measurement of rainfall at attenuating wavelengths. *J. Meteorol.*, 11, 58-67.

Houze, R. A., 1981: Structures of atmospheric precipitation systems: A global survey. *Radio Sci.*, 16, 671-689.

Ighuchi, T., and R. Meneghini, 1994: Intercomparison of single-frequency methods for retrieving a vertical rain profile from airborne of spaceborne radar data. *J. Atmos. Oceanic Technol.*, 11, 1507-1516.

Kedem, B., L. S. Chiu, and G. R. North, 1990: Estimation of mean rain rate: application to satellite observations. *J. Geophys. Res.*, 95, 1965-1972.

Kozu, T., and T. Iguchi, 1996: A preliminary study of non-uniform beam-filling correction for spaceborne radar rainfall measurement. *I.E.I.C.E. Trans. Comm.*, E79B, 763-769.

Kummerow, C., and L. Giglio, 1994: A passive microwave technique for estimating rainfall and vertical structure information from space. Part I: algorithm description. *J. Appl. Meteor.*, 33, 3-18.

Lopez, R. E., 1977: The log-normal distribution and cumulus cloud populations. *Mon. Wea. Rev.*, 105, 865-872.

Marzoug, M., and P. Amayenc, 1994: A class of single-frequency algorithms for rain-rate profiling from a spaceborne radar. 1. Principle and tests from numerical simulations. *J. Atmos. Oceanic Technol.*, 11, 1480-1506.

Meneghini, R., J. Eckerman, and D. Atlas, 1983; Determination of rain rate from a spaceborne radar using measurements of total attenuation, *IEEE Trans. Geosci. Remote Sensing*, 20, 34-43.

Nakamura, K., 1991: Biases of rain retrieval algorithms for spaceborne radar caused by nonuniformity of rain. *J. Atmos. Oceanic Technol.*, 18, 363-373.

Nakamura, K., K. Okamoto, T. Ihara, J. Awaka, T. Kozu, and T. Manabe, 1990: Conceptual design of rain radar for the tropical rainfall measuring mission. *Int. J. Satellite Comm.*, 8, 257-268.

Schroeder, L. C., P. R. Schaffner, J. L. Mitchell, and W. L. Jones, 1985: AAFE RADSCAT 13.9 GHz measurements and analysis: wind-speed signature of the ocean. *IEEE J. Oceanic Eng.*,10, pp. 346-357.

Figure Captions

1. Two-dimensional spaceborne radar beam as it intersects rain. The vertical axis is altitude and the horizontal axis is distance across the radar footprint.

2. Calculated NUBF errors (apparent minus true) for a lognormal rain rate. The error is shown as a function of the mean rain rate; the standard deviation of the rain rate within the footprint is equal to the mean rain rate. (a) PIA, and (b) near surface reflectivity. Solid line is perfect correlation, dashed line is independence.

3. ARMAR data from TOGA COARE, acquired January 18, 1993. Vertical axis is altitude (8km) and horizontal is along track distance (40 km). Reflectivity ranges from 10 dBZ (black) to 50 dBZ (white). White horizontal line is return from ocean surface. Upper image is original high resolution data; lower is result of TRMM PR simulation. Alignment between upper and lower is approximate.

4. Plots of quantities computed for the case in Figure 3. (a) True rain rate (solid), apparent rain rate (dashed). (b) Errors in PIA (solid), rain-rop reflectivity (dashed), and near-surface reflectivity (dotted).

5. Histogram of NUBF errors over the TOGA COARE experiment. Errors are always apparent relative to true; positive errors indicate that use of the apparent quantities causes overestimation relative to the true quantities. (a) PIA (solid), reflectivity at 4 km altitude (dashed), reflectivity near surface (dotted). (b) PARR (solid), rain rate at 4 km altitude (dashed), and rain rate near surface (dotted).

6. (a) Scatter plot of the PIA error versus the standard deviation of the high resolution path attenuation within the footprint. (b) Scatter plot of the error in reflectivity at 4 km altitude versus standard deviation of high resolution reflectivity at 4 km within the footprint.

7. Scatter plot showing relation between low-resolution observables and high resolution standard deviation.

Table 1: Comparison of ARMAR and TRMM PR Parameters

	ARMAR	TRMM
Frequency	13.8 GHz	13.8 GHz
Scanning swath	9 km	220 km
Scan angles	$\pm 20^o$	$\pm 17^o$
Surface horizontal resolution	800 m	4 km
Range resolution	100 m	250 m
Noise floor (at surface)	10 dBZ	23 dBZ
Samples	> 100	64

Table 2: Statistics of NUBF Errors (Apparent Minus True)

Parameter	Mean	Std. Dev.	Minimum	Maximum
PIA (dB)	-0.2	-0.8	-11.7	0.0
PARR (mm/h)	-0.4	1.4	-20.6	0.0
Rain-top Z (dBZ)	0.3	0.5	0.0	5.5
Rain-top R (mm/h)	0.06	0.14	0.0	2.3
Near-surface Z (dBZ)	0.0	0.7	-12.2	10.4
Near-surface R (mm/h)	-0.8	4.9	-78.8	17.6

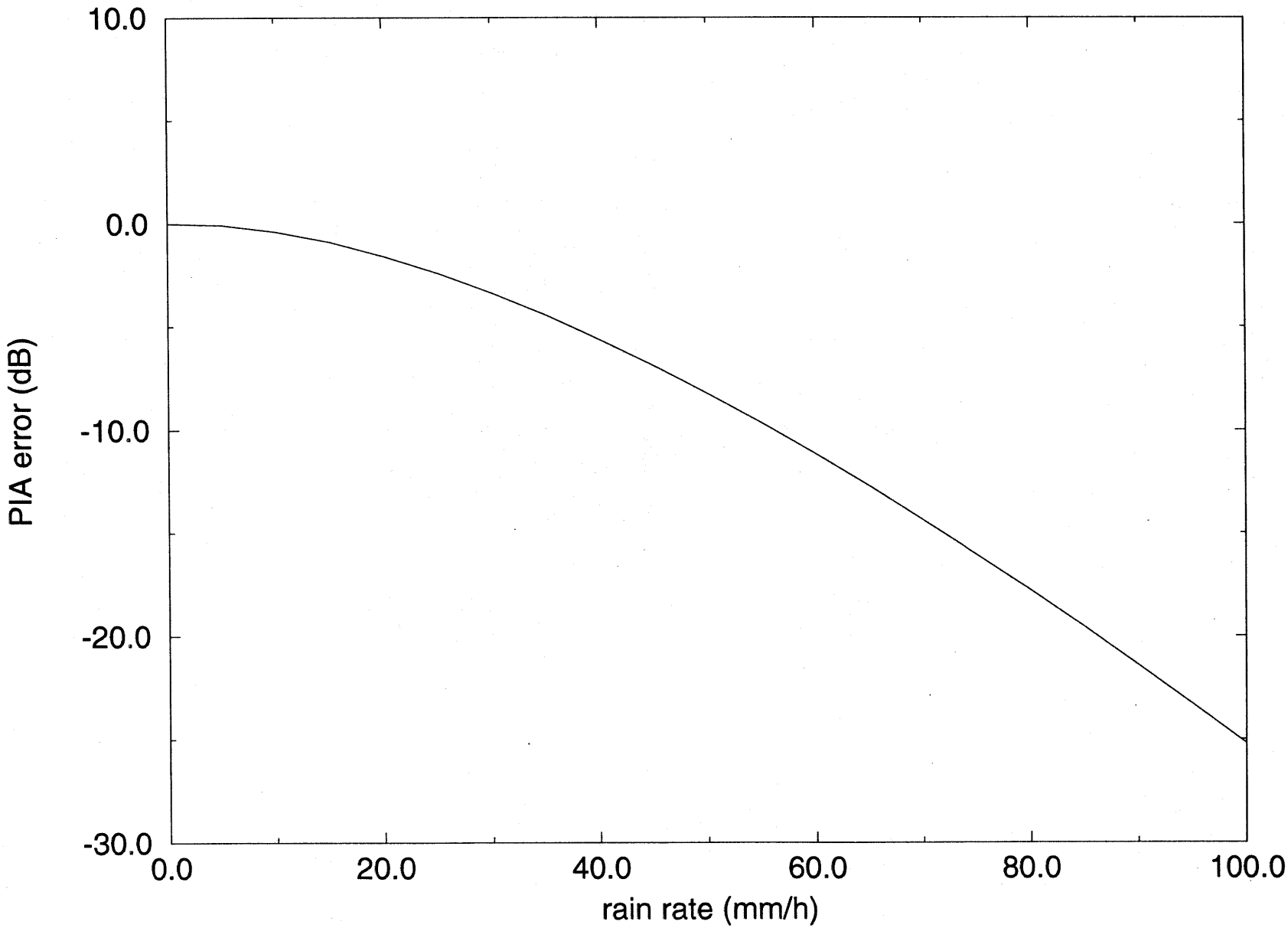
10.0
0.0
-10.0
-20.0
-30.0
PIA error (dB)
0.0
20.0
40.0
60.0
80.0
100.0
rain rate (mm/h)

2a

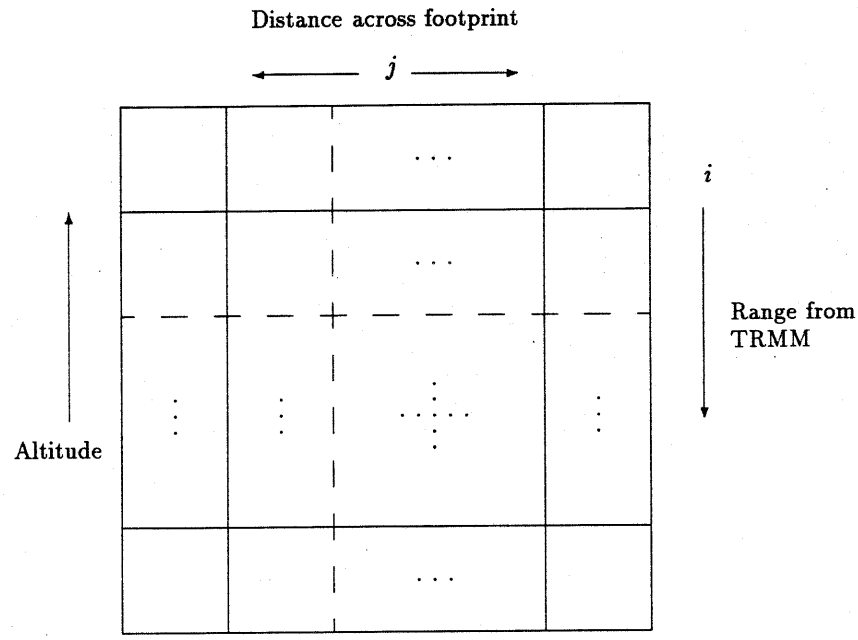

Figure 1

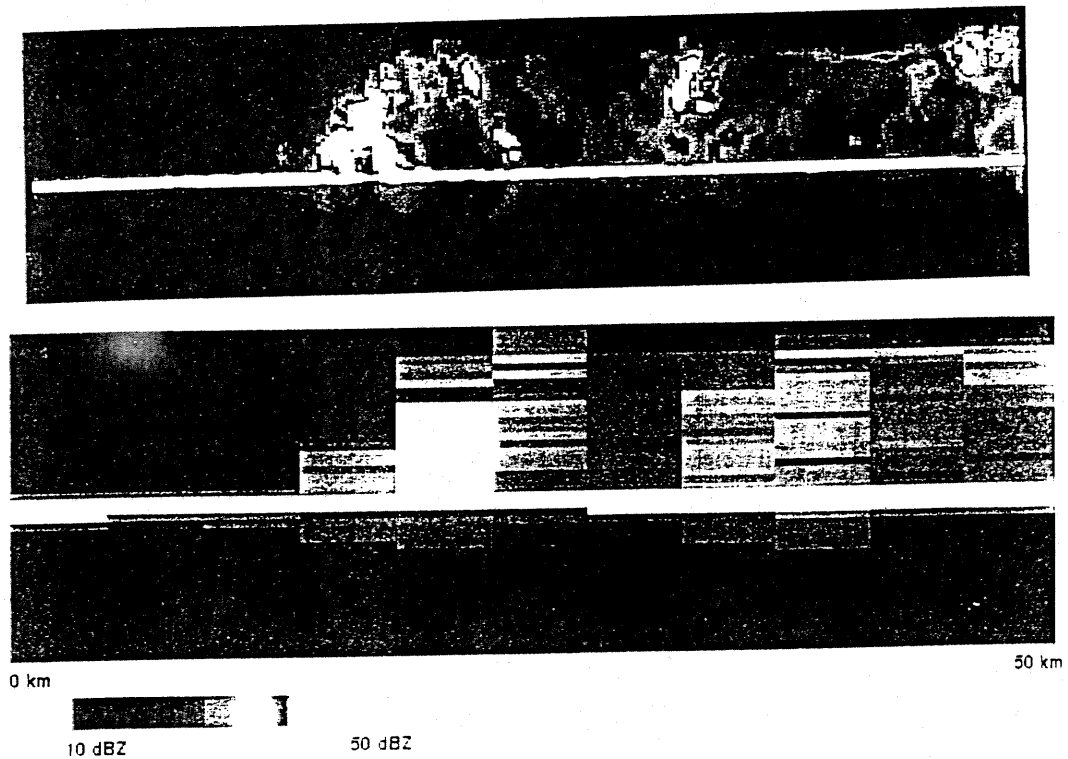

3

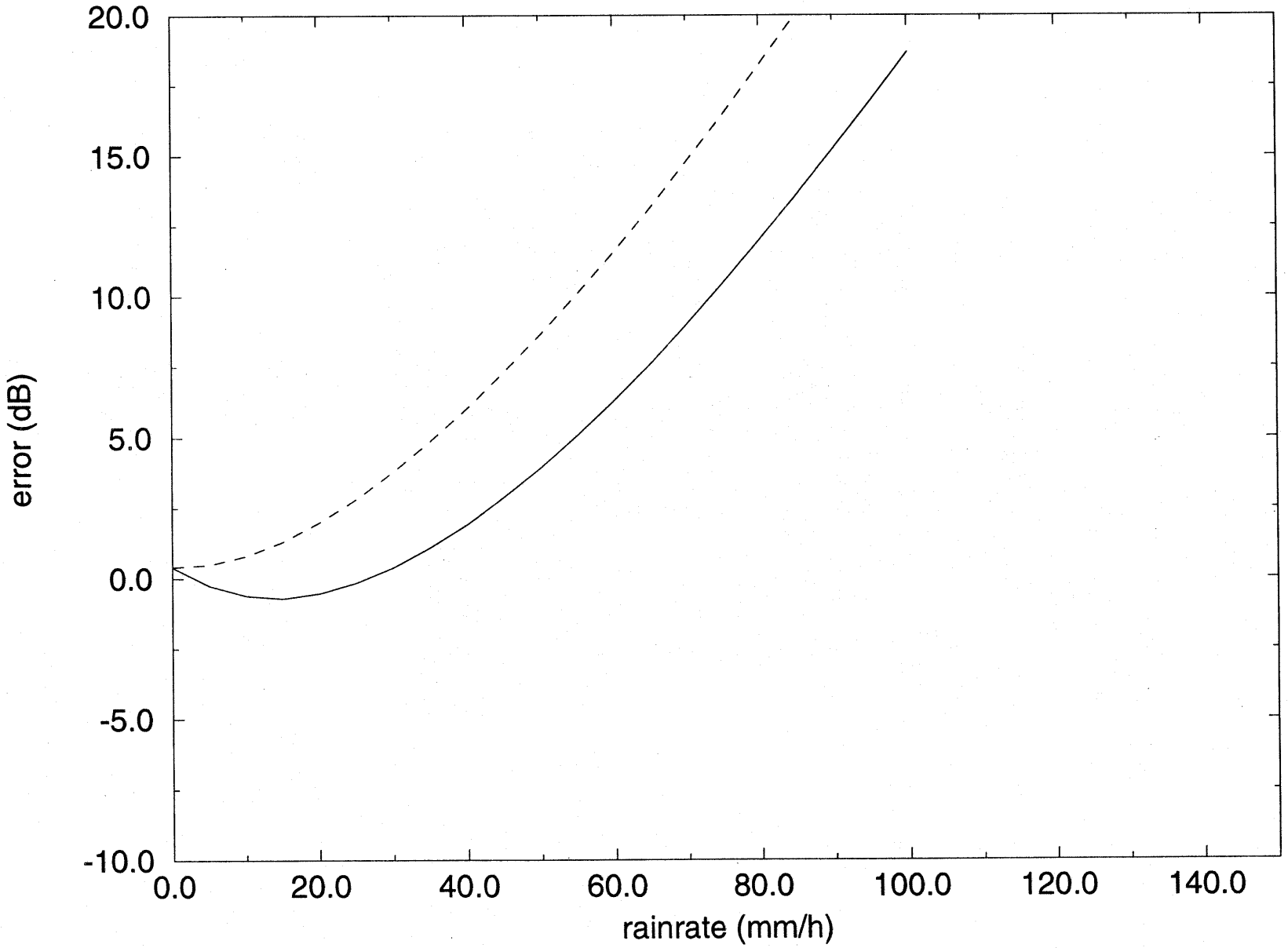
20.0
15.0
10.0
5.0
0.0
-5.0
-10.0
error (dB)
0.0
20.0
40.0
60.0
80.0
100.0
120.0
140.0
rainrate (mm/h)

2b

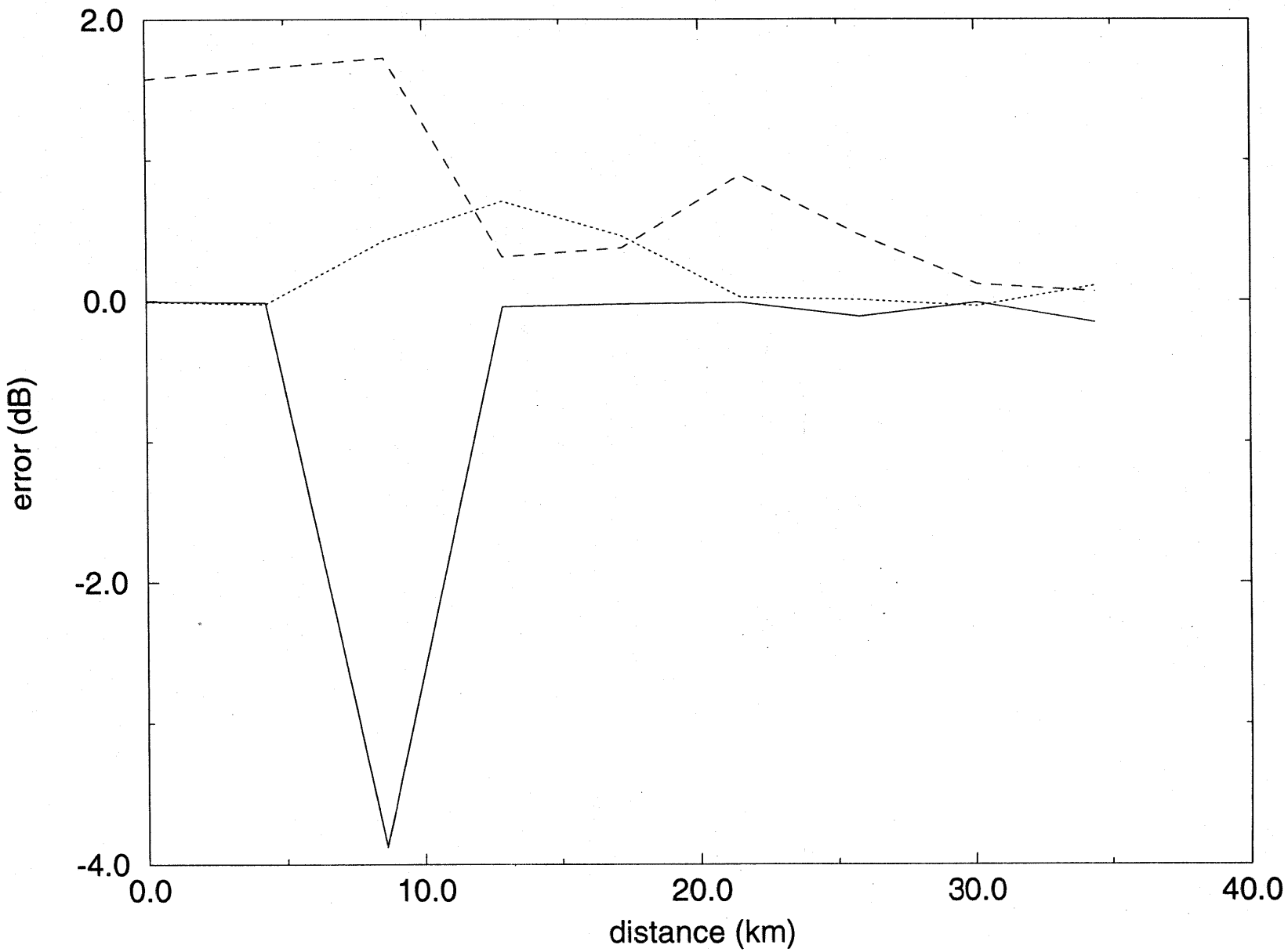

4b

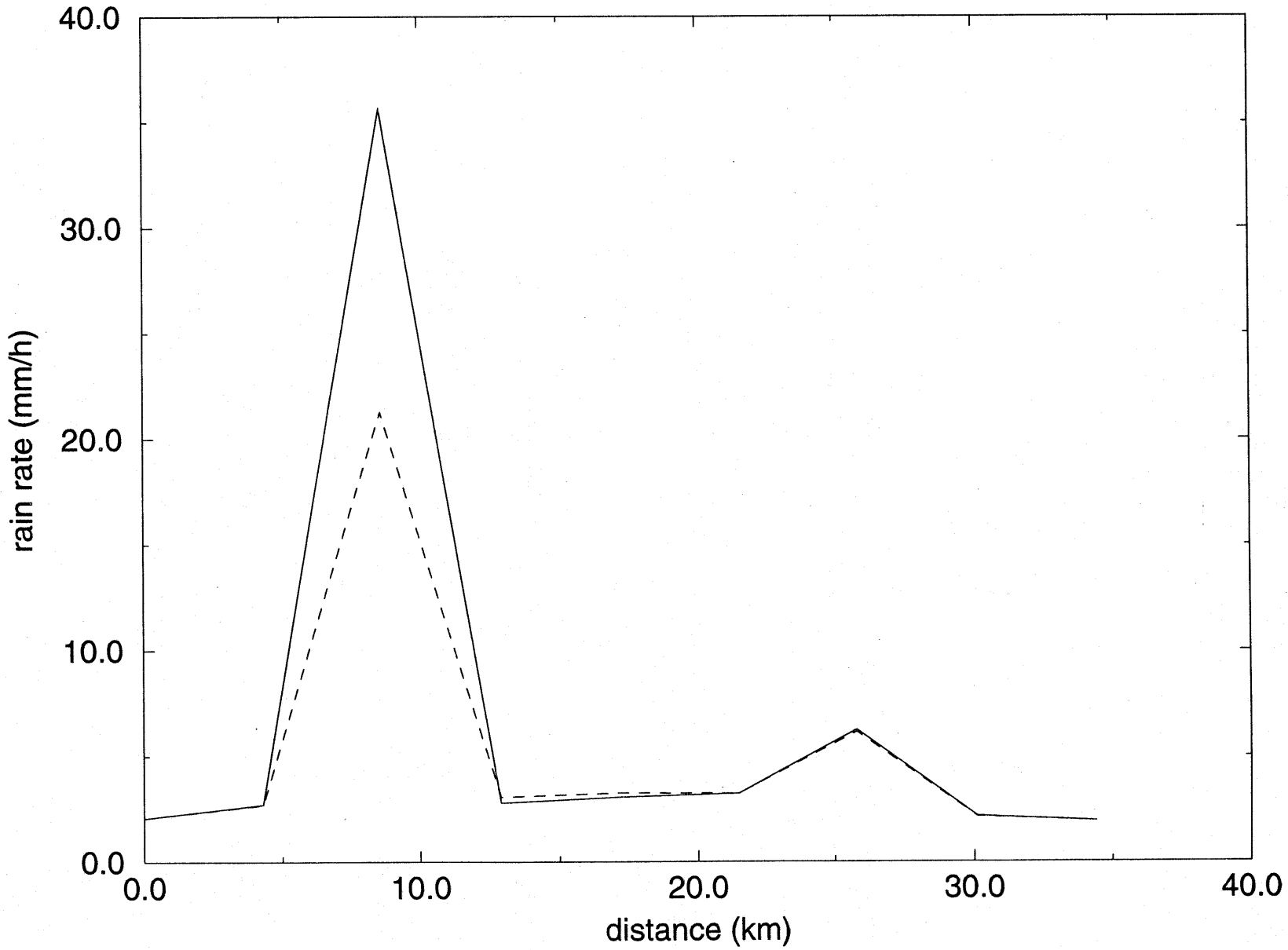

4 a

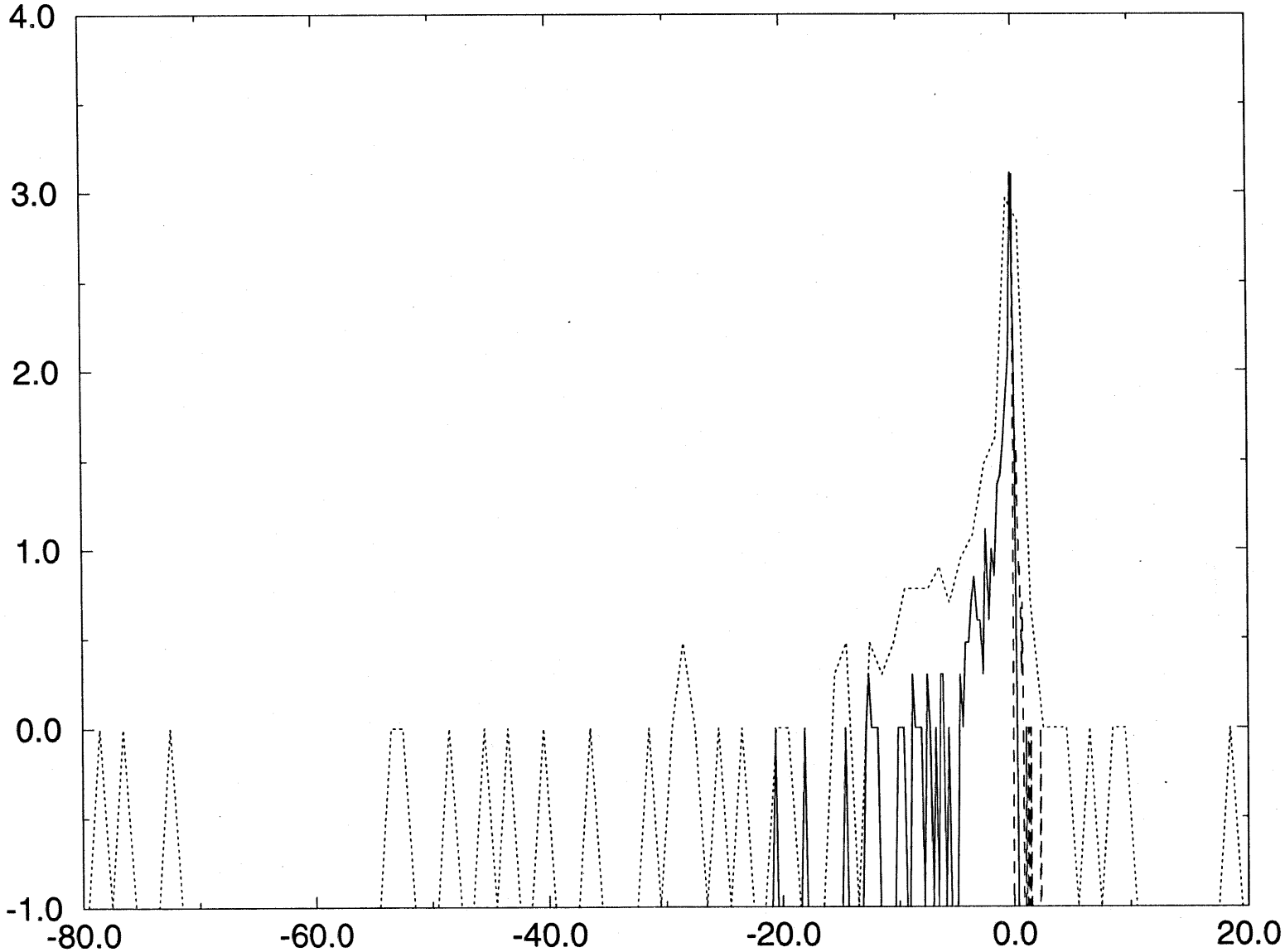
4.0
3.0
2.0
1.0
0.0
-1.0
-80.0
-60.0
-40.0
-20.0
0.0
20.0

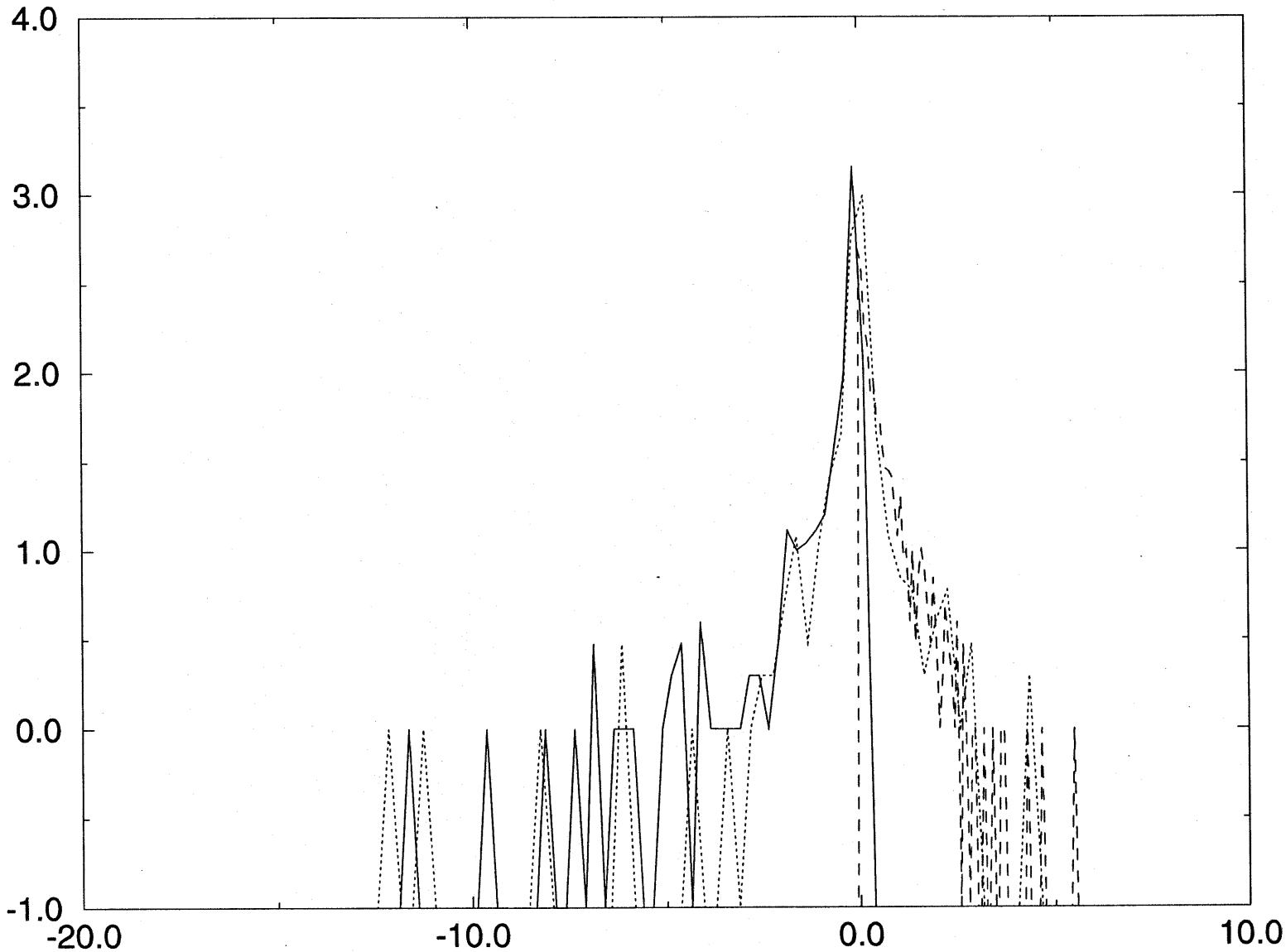

5 a

Z ESTIMATION ERROR

EFFECT OF Z VARIABILITY WITHIN CELL

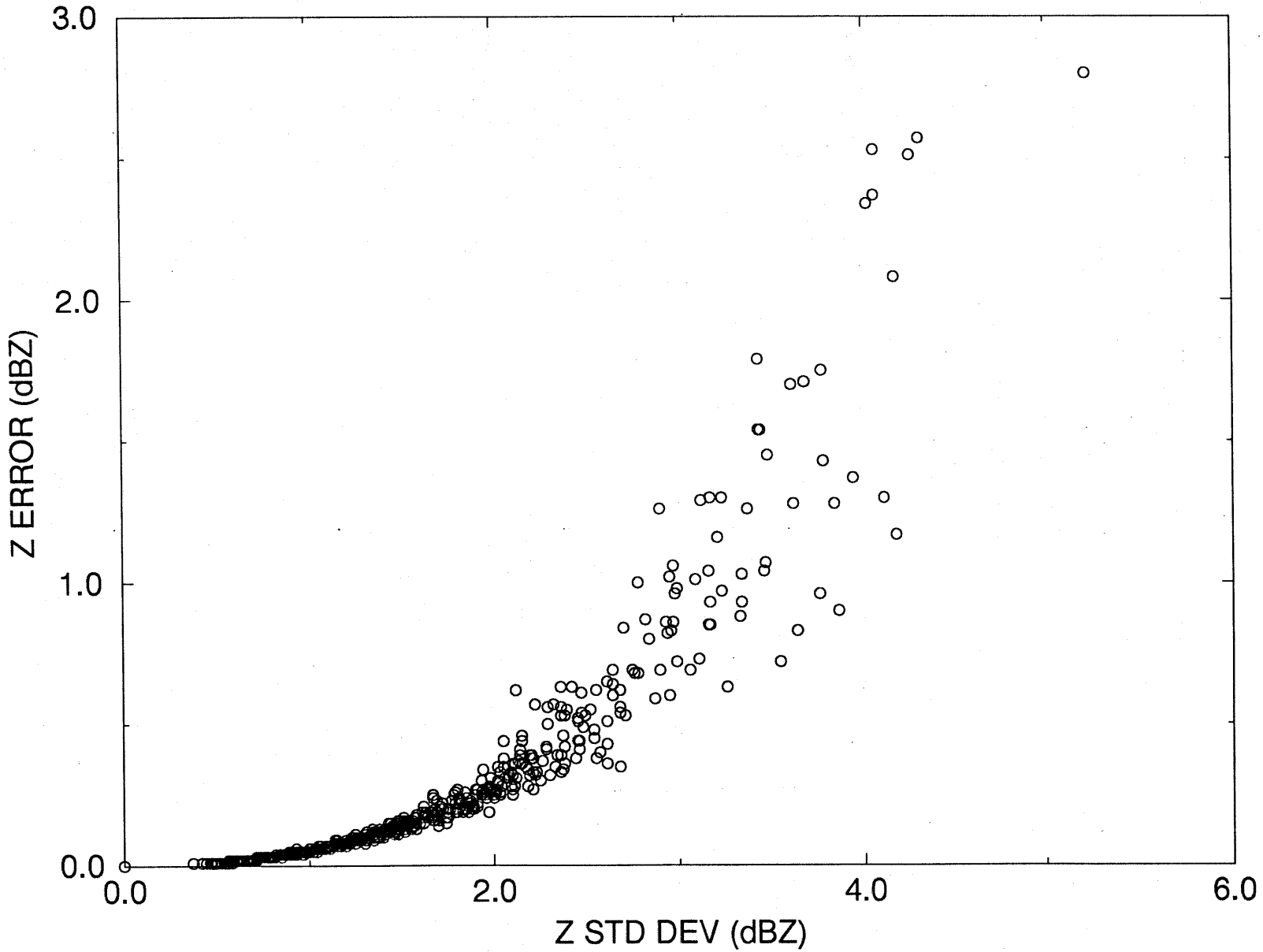

PIA ESTIMATION ERROR

EFFECT OF PIA VARIABILITY WITHIN FOOTPRINT

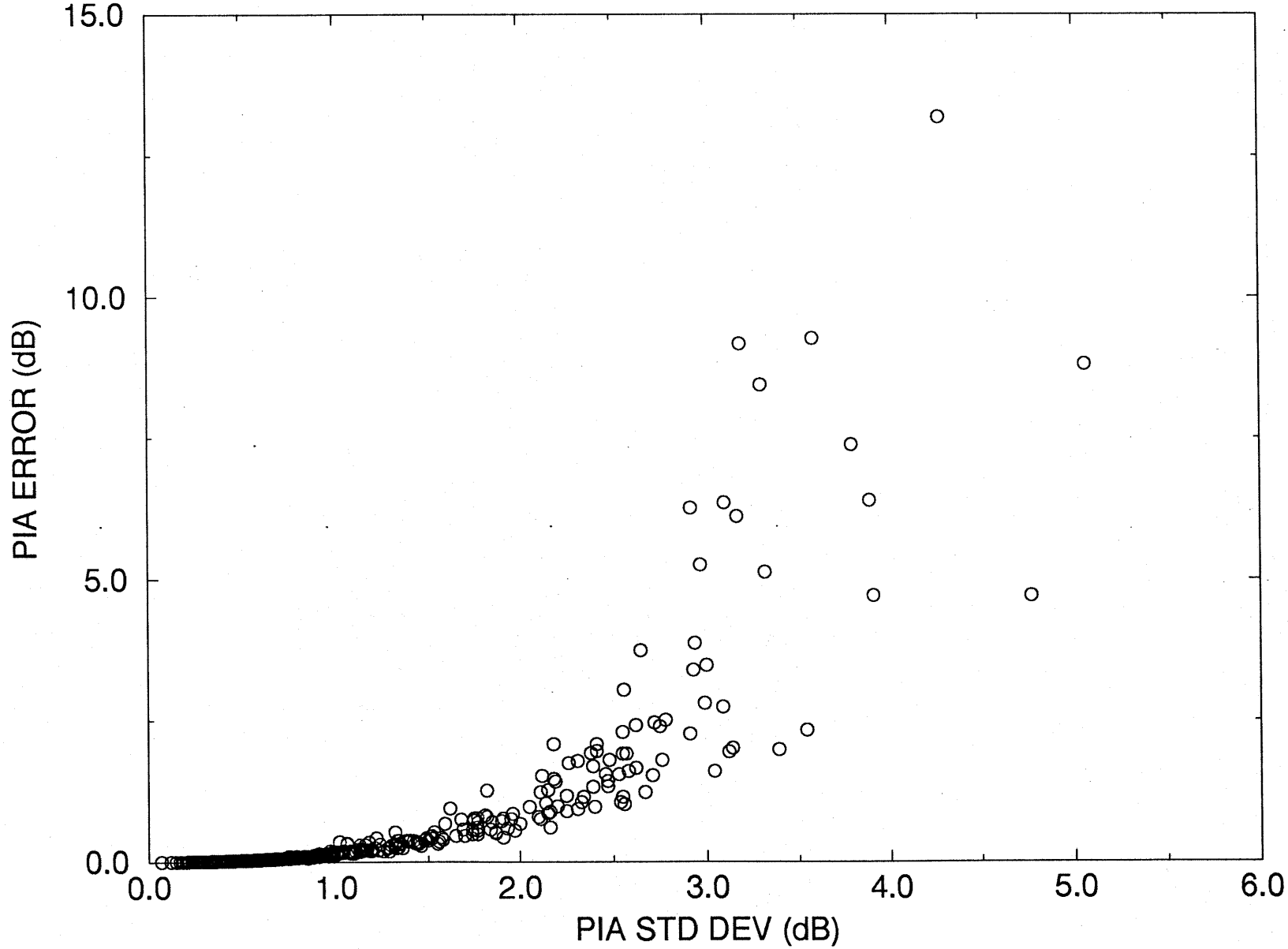

6a

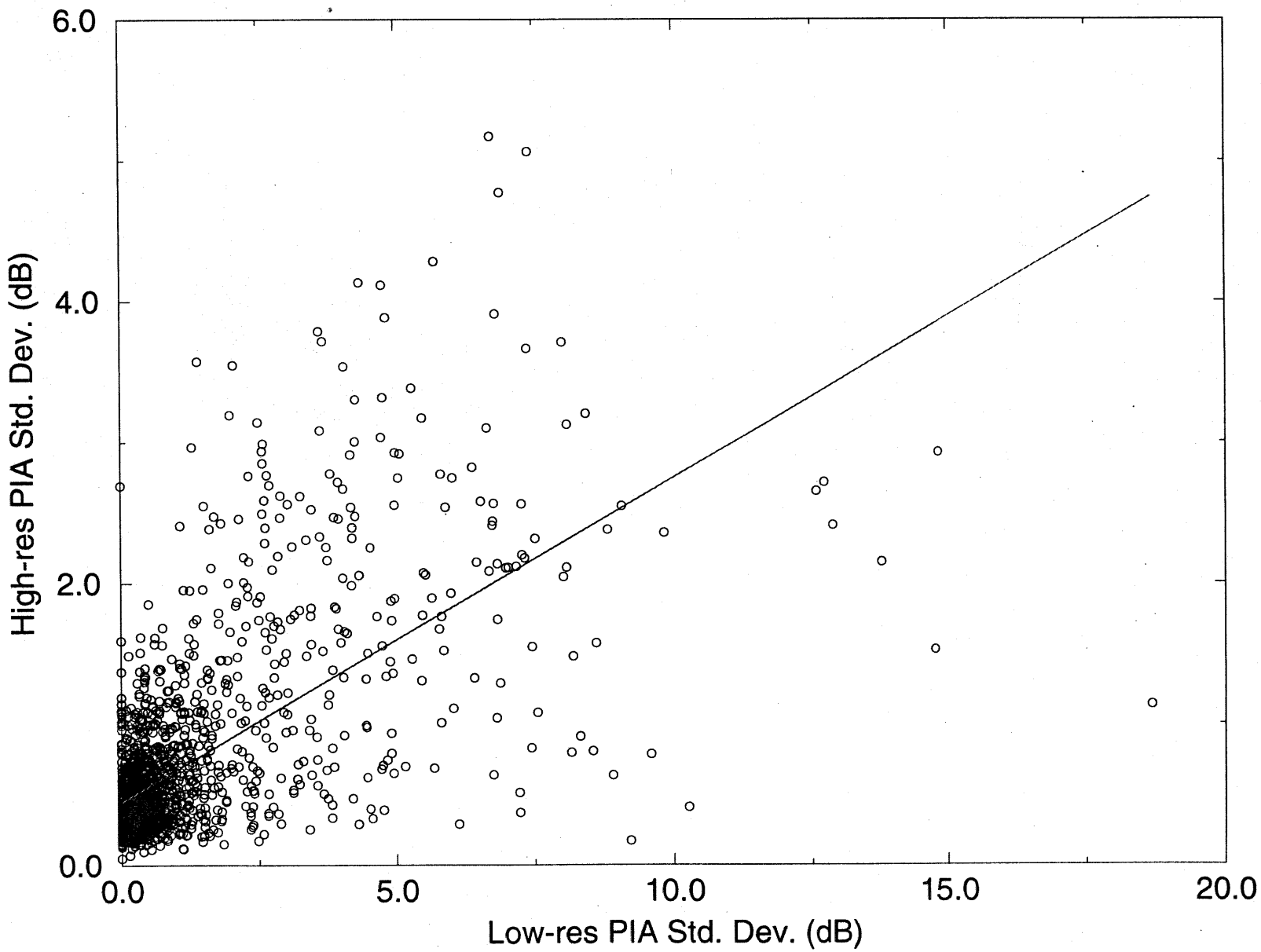
6.0
4.0
2.0
0.0
High-res PIA Std. Dev. (dB)
0.0
5.0
10.0
15.0
20.0
Low-res PIA Std. Dev. (dB)